Effect of Co Addition on the Microstructure, Martensitic Transformation and Shape Memory Behavior of Fe-Mn-Si Alloys

BIKAS C. MAJI, MADANGOPAL KRISHNAN, M. SUJATA, GOUTHAMA, and RANJIT K. RAY

The effect of Co addition has been studied in Fe-30Mn-6Si-xCo (x = 0 to 9 wt pct) shape memory alloys in terms of their microstructure, martensitic transformation and shape recovery. Microstructural investigations reveal that in Fe-Mn-Si-Co alloys, the microstructure remains single-phase austenite (γ) up to 5 pct Co and beyond that becomes two-phase comprising γ and off-stoichiometric $(Fe,Co)_5Mn_3Si_2$ intermetallic π-phases. The forward γ-ε martensite transformation start temperature (M_S) decreases with the addition of Co up to 5 pct, and alloys containing more than 5 pct Co, show slightly higher M_S possibly on account of two-phase microstructure. Unlike M_S, the ε-γ reverse transformation start temperature (A_S) has been found to remain almost unaltered by Co addition. In general, addition of Co to Fe-Mn-Si alloys deteriorates shape recovery due to decreasing resistance to plastic yielding concomitant with the formation of stress induced ε martensite. However, there is an improvement in shape recovery beyond 5 pct Co addition, possibly due to the strengthening effect arising from the presence of $(Fe,Co)_5Mn_3Si_2$ precipitates within the two-phase microstructure and due to higher amount of stress induced ε martensite.

DOI: 10.1007/s11661-012-1378-z

I. INTRODUCTION

THE shape memory effect (SME) associated with the austenite (γ)-ε martensitic transformation has been reported in a number of Fe-based alloy systems. Enami *et al.*[1] were the first to report SME in Fe-18.5 pct Mn binary alloy, although, the amount of shape recovery observed in this alloy was very limited. The extent of recovery in these binary Fe-Mn alloys improves with increasing Mn content up to 20 pct. However, at higher Mn contents (more than 23 wt pct) the parent γ-phase gets stabilized due to paramagnetic to anti-ferromagnetic transition.[2] It was Gartstein *et al.*[3] who first suggested that addition of ternary elements such as Si or Co can widen the temperature range of γ-ε transformation and increase the amount of ε martensite. They also pointed out that such ternary alloying will not substantially affect the martensite transformation start temperature (M_S) but will strongly reduce the paramagnetic to anti-ferromagnetic transition temperature, Néel transition temperature (T_N), of these alloys. Subsequent to that a few years later, Sato *et al.*[4] reported that addition of small amount of Si (~1 pct) in single-crystal Fe-30 pct Mn alloy can improve the shape recovery to a great extent. Based on this idea, Murakami *et al.*[5] developed the first polycrystalline Fe-Mn-Si shape memory alloys (SMAs), which could show recoverable strain more than 1.7 pct. Thereafter several studies have been carried out on these Fe-Mn-Si based SMAs to improve their recoverable strain by thermo-mechanical training,[6,7] corrosion resistance by alloying[8] and the strength of the γ-matrix either by solid solution[9] or precipitation hardening.[10,11] However, so far only a very limited numbers of studies are available in published literature on Fe-Mn-Co SMAs.

Hamers and Wayman[12] were the first to study the shape memory behavior of Fe-Mn-Co alloys in a limited composition range of Fe-(25-30)Mn-(5-8)Co and found that the amount of recovery in these alloys is comparatively lower than Fe-Mn-Si alloys. Contrary to their results, Reyhani *et al.*[13] studied the shape memory behavior in Fe-(14-26)Mn-9Co-5Ni alloys and concluded that the amount of shape recovery in these alloys is comparable to that of Fe-Mn-Si or Fe-Mn-Si-Cr-Ni SMAs. Jiang *et al.*[14] have examined the effect of Co addition on the martensitic transformation and shape recovery of Fe-Mn-Si-Cr-Ni alloys. These authors[14] have reported that Co addition lowers the stacking fault energy of these alloys and leads to an increase in M_S temperature for γ-ε transformation. They have also shown that the amount of shape recovery in these alloys could be enhanced by adding optimal amount of Co. The composition dependence of the γ-ε transformation in Fe-Mn-Co alloys has been modeled by Baruj *et al.*[15,16] Their studies reveal that low amount of Co addition (less than 10 pct) has very limited effect on the

BIKAS C. MAJI and MADANGOPAL KRISHNAN, Scientific Officers, are with the Materials Science Division, Bhabha Atomic Research Centre, Mumbai 400 085, India. Contact e-mail: bikchan@barc.gov.in M. SUJATA, Scientist, is with the Materials Science Division, National Aerospace Laboratories, Bangalore 560 017, India. GOUTHAMA, Professor, is with the Department of Materials Science and Engineering, Indian Institute of Technology, Kanpur, Kanpur 208 016, India. RANJIT K. RAY, Visiting Scientist, is with the R & D Division, Tata Steel, Jamshedpur 831 007, India.

Manuscript Submitted February 23, 2012.
Article published online August 30, 2012

martensitic transformation of Fe-Mn alloys. Based on the previously published literature, it is clearly evident that there is lot of discrepancy on the effect of Co addition on the γ-ε martensitic transformation and shape recovery of Fe-based SMAs and possibly the exact role it plays has also not been understood properly.

Although a few studies are already available in published literature on the shape memory behavior of ternary Fe-Mn-Co alloys, there is a lack of any systematic studies on the shape memory behavior of quaternary Fe-Mn-Si-Co alloy system. Thus, in the present study an attempt has been made to understand the effect of Co addition on the microstructure, martensitic transformation and shape memory behavior of Fe-Mn-Si alloys. For this purpose a series of Fe-Mn-Si-Co alloys have been created by systematically adding Co to a Fe-30Mn-6Si base alloy, which shows more than 90 pct shape recovery as reported by Murakami *et al.*[5]

II. EXPERIMENTAL

The nominal compositions of the alloys used for the present study are given in Table I. Alloy buttons were prepared by non-consumable vacuum arc melting using high purity (99.95 pct) alloying elements (Fe, Mn, Si and Co). The arc melted buttons were hot rolled at 1223 K (950 °C) into strips of 0.5 mm thickness and Table I gives a summary of their hot rollability. Hot rolled strips were further sealed in quartz capsules and solution annealed at 1323 K (1050 °C) for 1 hour. At the end of the solutionization treatment specimens were directly quenched into a water bath by breaking the quartz capsules. These solutionized materials were used for microstructural characterization and evaluation of shape memory property.

Optical microscopy, X-ray diffraction (XRD) and scanning electron microscopy (SEM) techniques were employed for microstructural characterization. Specimens used for the optical and SEM studies were mechanically ground and polished up to 1 μm surface finish and the microstructures were revealed by etching with a 5 pct Nital solution. XRD analysis was carried out using Mo-k_α radiation ($\lambda_{k\alpha 1}$ = 0.7093 Å) to identify and quantify the phase constituents. The chemical compositions of constituent phases were determined by wavelength dispersive spectrometry (WDS) attached to an electron probe micro analyzer (EPMA) and energy dispersive spectrometry (EDS) attached to a SEM. The electron back scatter diffraction (EBSD) measurements were conducted at 20 kV acceleration voltage with a step size of 0.1 μm on a field emission gun (FEG) source FEI Quanta 3D SEM equipped with TSL-OIM™ EBSD set-up. The characteristic martensite transformation temperatures (start and finish) were measured using a differential scanning calorimeter (DSC; DSC 822e, METTLER-TOLEDO, Switzerland) at a heating/cooling rate of 10 K/minute. All DSC measurements were carried out on specimens of about 50 to 60 mg in weight. The shape memory property was evaluated by a simple bend test, details of which are given in Reference 17. The amount of recovery was determined by applying a pre-strain between 2 to 8 pct at room temperature followed by a recovery annealing at 873 K (600 °C) temperature for 10 minutes. The percentage recovery was calculated on the basis of change in angular distance of the pre-strained specimens before and after recovery. Room temperature tensile tests were performed at a strain rate of 6.7×10^{-4} in an electromechanical tensile testing machine using 0.5 mm thick tensile specimens of 12.5 mm gage length.

Table I. Nominal Alloy Compositions

Alloy	Nominal Compositions (mass pct) Mn	Si	Co	Fe	Hot Rollability
0Co	30	6	0	64	successful
1Co	30	6	1	63	successful
3Co	30	6	3	61	successful
5Co	30	6	5	59	successful
7Co	30	6	7	57	successful
9Co	30	6	9	55	successful

III. RESULTS

A. *Microstructure After Solution Annealing*

Figure 1 presents the optical micrographs of alloys 0Co to 9Co after solution annealing at 1323 K (1050 °C). These micrographs essentially reveal that alloys with 0 to 5 pct Co (alloys 0Co to 5Co) essentially have a single-phase austenite (γ) microstructure and alloys containing more than 5 pct Co (alloys 7Co and 9Co) are composed of γ and a second phase that occurs mostly along grain boundaries. The amount and size of this second-phase increases with the Co content (alloys 7Co and 9Co). Apart from these phases, ε martensite is also observed in all alloys. This ε martensite phase (darker regions) appears as parallel plates within γ grains and normally forms on water quenching. Some amounts of annealing twins, which are common in austenitic stainless steels, were also noticed in these microstructures.

The XRD patterns obtained from solution treated alloys are shown in Figure 2. Apart from the reflections of the *fcc* γ and *hcp* ε martensite phases, the patterns show an additional low intensity peak at 2θ = 20.22 that matches well with the (011) reflection of *bcc* α' martensite/δ-ferrite (with lattice parameter a = 0.286 nm). It is possible that a small amount of α' martensite or δ-ferrite phase may be present in these microstructures. On the other hand, the XRD patterns of alloys 7Co and 9Co, which have a two-phase microstructure, do not show any reflection of the second-phase even though they are clearly visible in the optical micrographs (Figures 1(e) and (f)). The absence of reflections can be due to the volume fraction of the phase being below the limit that can be detected in XRD, or else due to loss of the grain boundary phase during specimen preparation (it has been observed to easily fall off during polishing). Quantitative Rietveld phase analysis[18] using

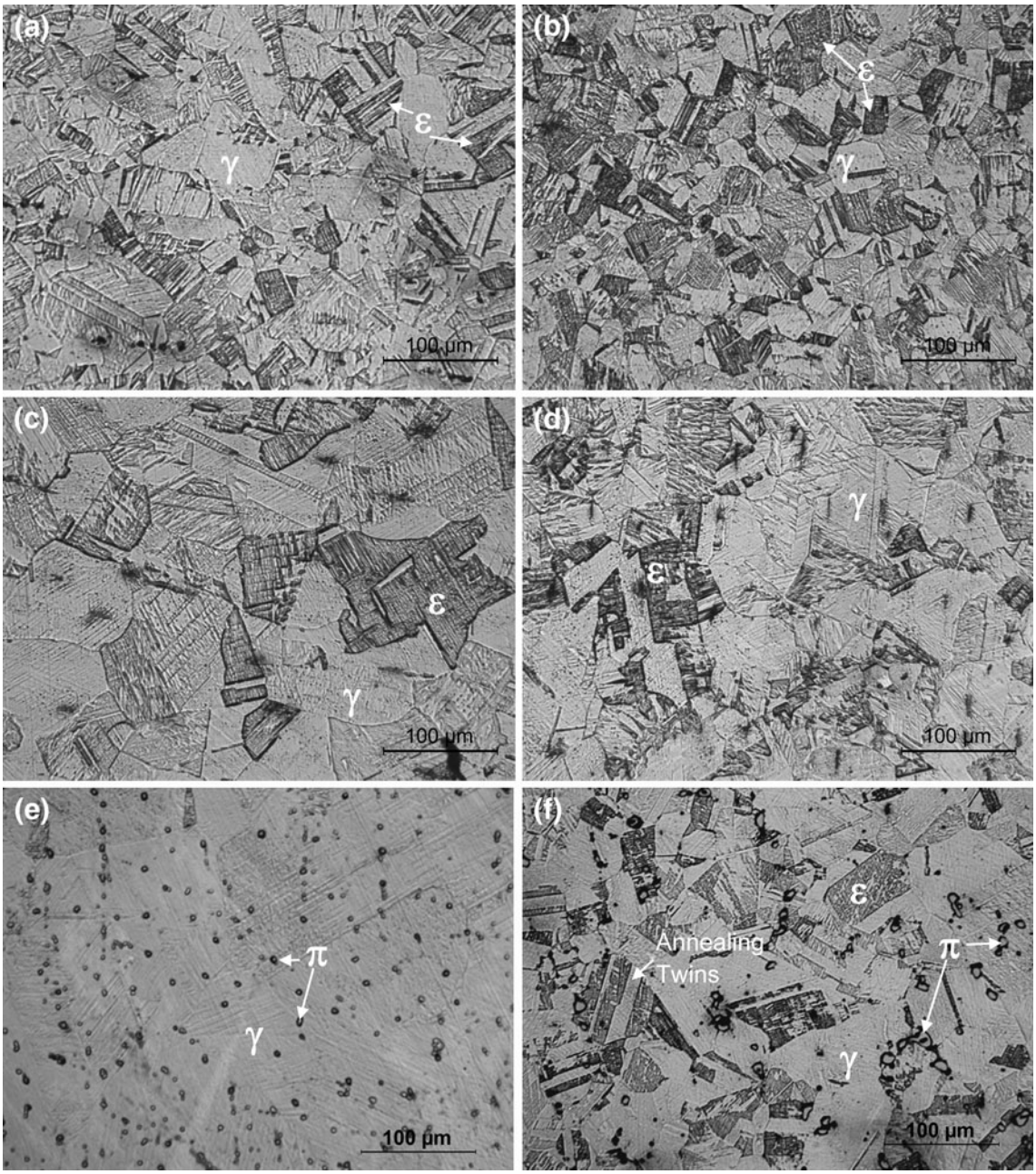

Fig. 1—Optical micrographs taken from 1323 K (1050 °C) solution annealed specimens of (*a*) 0Co, (*b*) 1Co, (*c*) 3Co and (*d*) 5Co alloys showing single-phase γ microstructure. The micrographs obtained from specimens (*e*) 5Co and (*f*) 9Co alloys show a two-phase microstructure composed of γ and $(Fe,Co)_5Mn_3Si_2$ intermetallic π-phase. Apart from these phases, some amount of athermal ε martensite and annealing twins are also seen to be present within these microstructures.

TOPAS software was employed to determine the lattice parameters and volume fractions of the constituent phases in solution treated alloys and are presented in Table II. It can be seen that the amount of athermal martensite is more or less the same in all alloys, *i.e.*, the amount of athermal martensite is unaffected by the addition of Co.

The microstructures of the solution treated alloys were examined at a finer scale by SEM. A thorough examination of the microstructure did not show the presence of α' martensite, Figure 3(a), which usually appears in lenticular shape[19] within ε martensite bands. An attempt to reveal α' martensite was also made using EBSD phase mapping. Figure 4 shows the typical EBSD maps generated from alloys 0Co and 1Co using structural data of γ, ε and α' martensite phases. It can be seen that these maps do not show the occurrence of α' martensite within ε plates. Therefore, the extra XRD reflection observed in Figure 2 (at $2\theta = 20.22$) is possibly due to the presence of some discrete δ-ferrite particles present in these alloys.

The semi-quantitative chemical analysis of the second phase precipitates, as shown in Figure 3(b), and the matrix was carried out by EDS (point analysis) and the results are presented in Table III. Figure 3(c) shows a

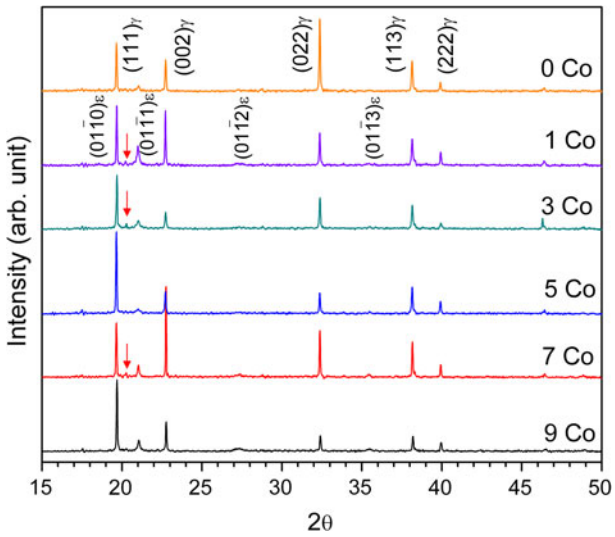

Fig. 2—XRD patterns obtained from 1323 K (1050 °C) solution annealed specimens reveal that the microstructures of these alloys are mainly comprised of γ and ε martensite. The existence of a minor peak (shown by an arrow) at $2\theta = 20.22$ position is possibly due to the presence of some amount of *bcc* δ-ferrite/α' martensite within the microstructures.

Table II. Lattice Parameters and Quantitative Phase Analysis

Alloy	Phase	Lattice Parameters (nm)	Volume Fraction (pct)
0Co	γ	$a = 0.360247$	77.73
	ε	$a = 0.255609$, $c = 0.410333$	22.27
	α'	–	–
1Co	γ	$a = 0.360142$	66.41
	ε	$a = 0.255607$, $c = 0.410089$	31.06
	α'	$a = 0.285553$	2.53
3Co	γ	$a = 0.360319$	75.06
	ε	$a = 0.255919$, $c = 0.408753$	22.32
	α'	$a = 0.285594$	2.62
5Co	γ	$a = 0.359984$	70.60
	ε	$a = 0.255672$, $c = 0.409328$	26.60
	α'	$a = 0.285409$	2.80
7Co	γ	$a = 0.359983$	73.91
	ε	$a = 0.254657$, $c = 0.411653$	25.44
	α'	$a = 0.285398$	0.65
9Co	γ	$a = 0.359889$	69.61
	ε	$a = 0.254619$, $c = 0.411574$	30.04
	α'	$a = 0.285612$	0.35

typical EDS spectra obtained from the second phase, which demonstrates that all alloying elements of the matrix such as, Fe, Mn, Si and Co are present in the second-phase. However, the amount of Si in the second-phase is almost double that of the γ matrix. The chemical compositions were also estimated by more precise EPMA-WDS technique and are shown in Table III. The EPMA analysis shows that, in single-phase alloys, the observed composition of the matrix γ phase agrees closely with the targeted alloy composition (Table I). However, the difference in the γ matrix composition of two-phase alloys (alloys 7Co and 9Co)

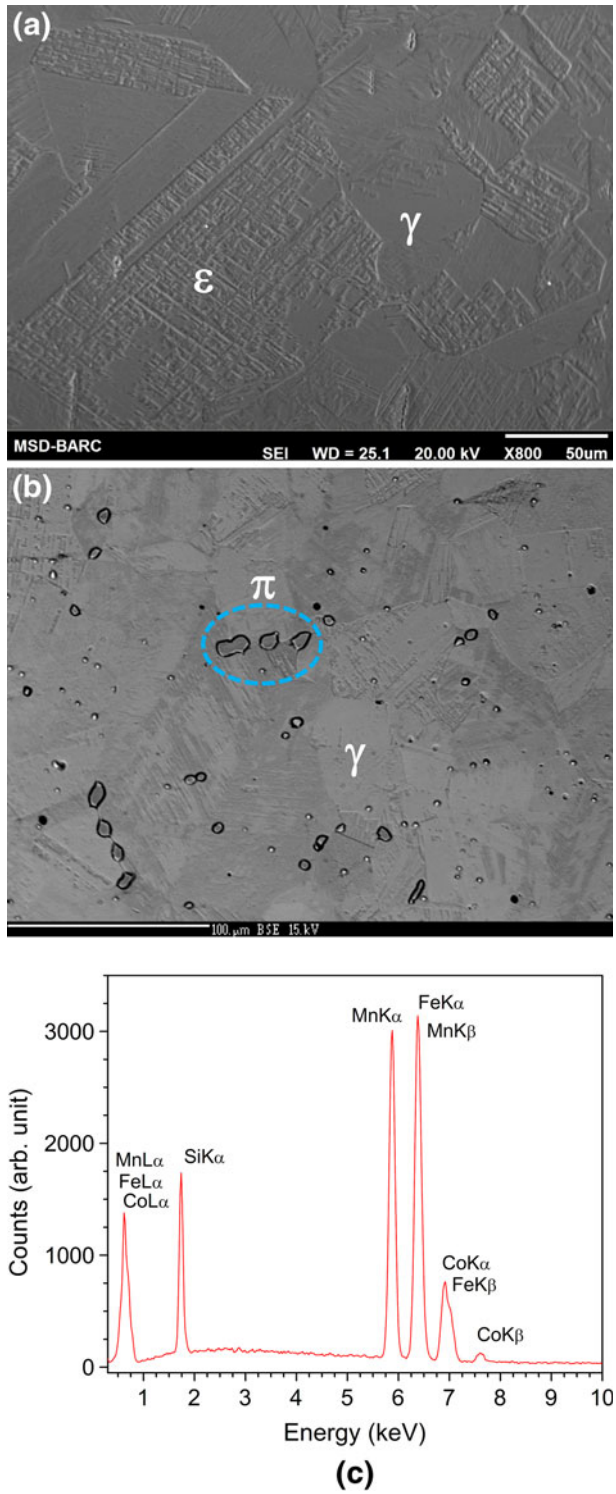

Fig. 3—(*a*) Scanning electron micrograph taken from solution annealed specimen of alloy 1Co shows that no α' martensite is present within the ε martensite colonies. The micrograph obtained from alloy 9Co (*b*) showing the presence of π-phase precipitates and (*c*) the corresponding EDS spectra reveals that these precipitates contain all alloying elements (Fe, Mn, Si and Co) similar to the γ matrix.

with respect to the targeted alloy composition is not high despite the presence of second phase precipitates (this may be due to the small volume fraction of the

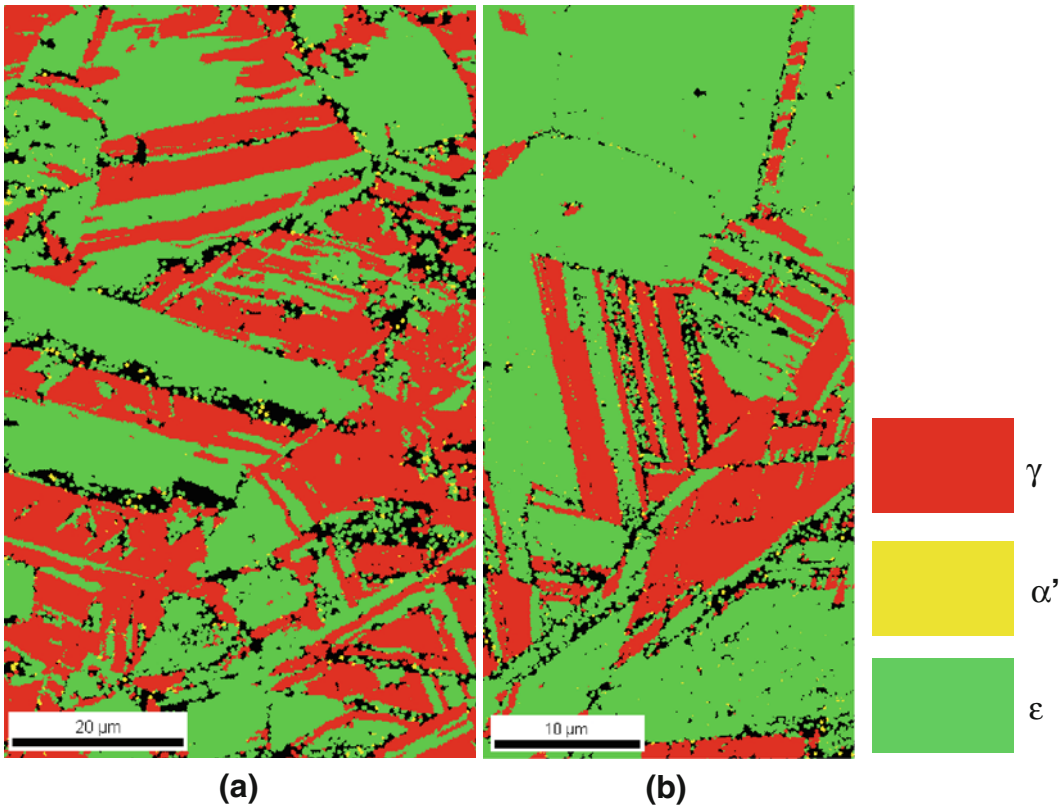

Fig. 4—EBSD phase maps obtained from alloy (*a*) 0Co and (*b*) 1Co after 1323 K (1050 °C) solution annealing show the presence of thermally induced ε martensite bands inside the γ grains. The occurrence of α′ martensite within ε martensite bands has not been detected in these phase maps (Color figure online).

Table III. Chemical Compositions of Constituent Phases

Alloys	Measurement Technique	Phases	Composition (mass pct)			
			Co	Mn	Si	Fe
0Co	WDS	γ	0	31.874	5.612	62.514
1Co	WDS	γ	0.824	29.669	6.289	63.218
3Co	WDS	γ	2.859	30.807	6.366	59.968
5Co	WDS	γ	4.950	31.439	6.026	57.585
7Co	WDS	γ	6.997	30.389	5.780	56.834
9Co	WDS	γ	8.788	30.145	6.235	54.832
	WDS	$(Fe,Co)_5Mn_3Si_2$	11.803	34.283	10.916	42.998
		at. pct	10.10	31.47	19.60	38.83
	EDS	γ	10.63	28.95	6.50	53.92
	EDS	$(Fe,Co)_5Mn_3Si_2$	13.43	33.48	10.34	42.75
		at. pct	11.56	30.92	18.67	38.85

precipitate). Table III shows that the second-phase is richer in Si, Co and Mn, as compared to the γ matrix, and leaner in Fe. It can also be seen that the ratio of (Fe + Co): Mn: Si in the second-phase is 48.93:31.47:19.60 (in at. pct), which is close to that the ratio of Fe:Mn:Si in the stoichiometric $Fe_5Mn_3Si_2$ intermetallic phase observed in Fe-Mn-Si alloys. This indicates that the precipitates may be off-stoichiometric $Fe_5Mn_3Si_2$ type intermetallic phase in which the Fe atom is partially substituted by Co. As the volume fraction of the phase was not high, the unambiguous identification of the phase by XRD was not possible. However, it was possible to obtain a more conclusive identification of the phase by EBSD analysis (Section III–E). It was also not possible to unambiguously determine the composition of the second phase in 7Co alloy by EPMA due to its small size. However, the EDS line scans across the precipitates suggests that these precipitates are in all likelihood the same as that of alloy 9Co.

B. *Transformation Behavior of the Solution Annealed Specimens*

The effect of Co addition on the transformation behavior of the solutionized alloys is shown in Figure 5

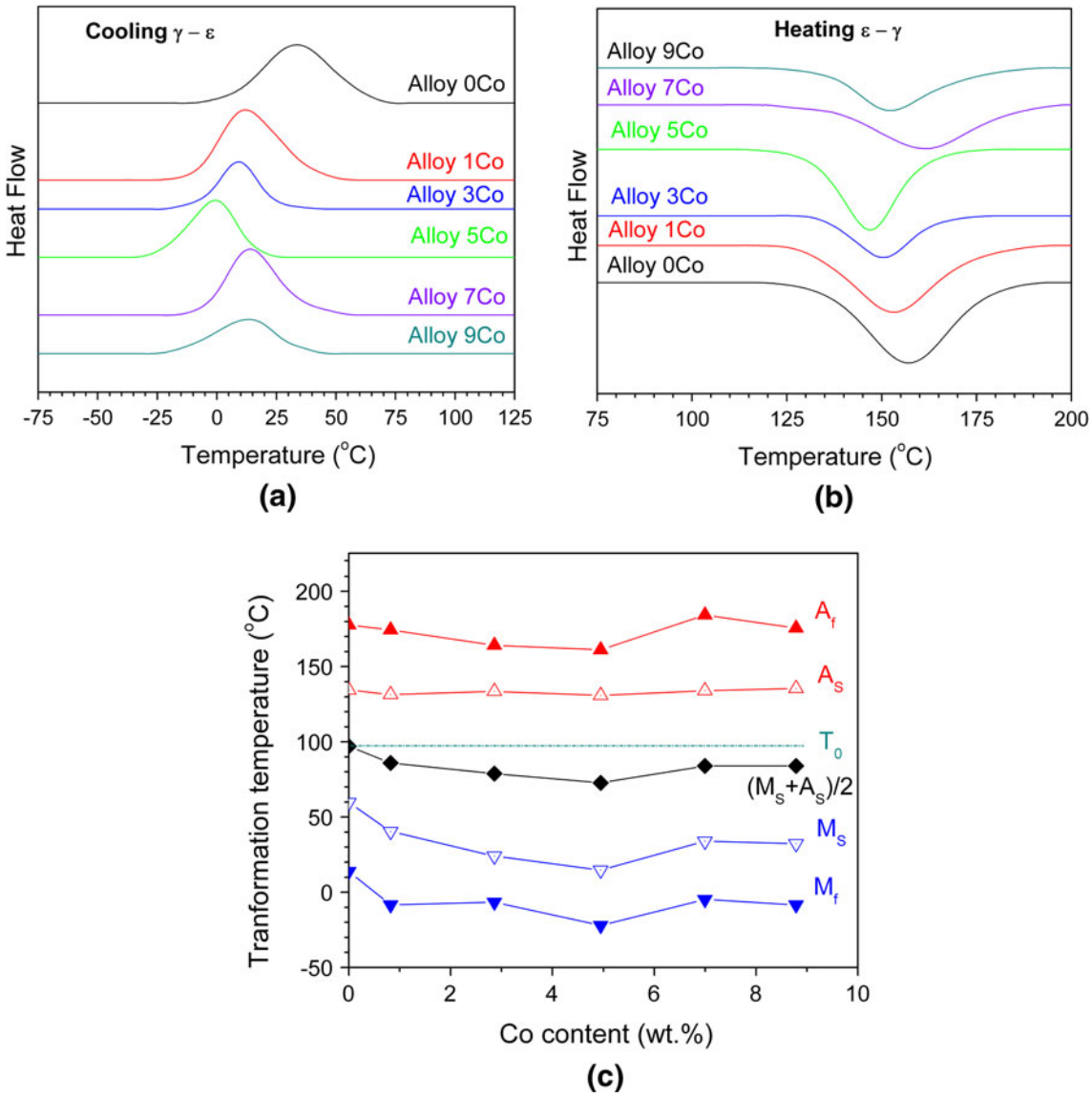

Fig. 5—The change in characteristic martensite transformation temperatures due to Co addition: (*a*) γ-ε forward transformation during cooling; (*b*) ε-γ reverse transformation during heating; and (*c*) as a function of Co content in these alloys.

Table IV. Martensitic Transformation Temperatures

Alloys	M_S (°C)	M_f (°C)	A_S (°C)	A_f (°C)	$\Delta H(\varepsilon\text{-}\gamma)$ (J/gm)	$\Delta T = (A_S - M_S)$	$(T_0 - M_S)$*	$(A_S - T_0)$*
0Co	59.58	13.79	134.39	177.71	1.13	74.81	37.41	37.40
1Co	40.45	−8.42	131.48	174.32	2.01	91.03	56.54	34.49
3Co	24.05	−6.62	133.57	164.17	1.01	109.52	72.94	36.58
5Co	14.73	−22.07	130.76	161.21	1.46	116.03	82.26	33.77
7Co	33.91	−4.78	134.04	184.24	1.22	100.13	63.08	37.05
9Co	32.25	−8.44	135.56	175.63	1.03	103.31	64.74	38.57

*Assuming $T_0 = (59.58 + 134.39)/2 = 96.99$ and remains unaffected with Co addition.

and the observed temperatures of the forward γ-ε martensitic transformation and reverse ε-γ phase transformation are presented in Table IV. In order to avoid quenching stresses affecting the transformation temperatures, the specimens were initially heated up to 473 K (200 °C) and then taken through the following cycle at a heating/cooling rate of 10 K/minutes: 473 K to 198 K to 473 K (200 °C to −75 °C to 200 °C). Figure 5(c) shows that the γ-ε martensite transformation start temperature (M_S) decreases till about 5 pct Co addition, and alloys with more (alloys 7Co and 9Co) show slightly higher M_S. Accordingly, the transformation hysteresis

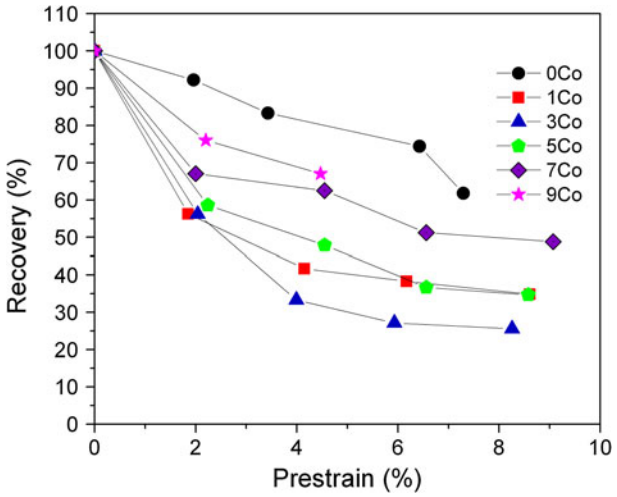

Fig. 6—Effect of Co addition on the shape recovery of Fe-Mn-Si alloys. Addition of Co has been observed to deteriorate the amount of recovery in these alloys.

($\Delta T = A_S - M_S$) of the alloys increases and then decreases. This behavior is possibly related to the fact that alloys 7Co to 9Co have two-phase microstructure, whereas alloys 0Co to 5Co have a single-phase austenitic microstructure. It also appears that the M_S temperature remains constant in the composition range with two-phase microstructure. Unlike M_S, the ε-γ reverse transformation start temperature (A_S) was found to remain almost unaltered by Co addition. The γ-ε martensitic transformation finish temperature (M_f) and ε-γ reverse transformation finish temperature (A_f), on the other hand, follow a trend similar to that of the M_S temperature.

C. *Shape Recovery of Solutionized Specimens*

Figure 6 shows the change in shape recovery due to Co addition, as measured by bend test. The recovery plots show that Co addition leads to drastic changes in the shape memory behavior. The amount of recovery was found to drop sharply, even with the slightest introduction of Co. This may either be due to the enhancement of irreversible plastic deformation (through reduction in the resistance to plastic yielding) or the increased formation of α' martensites in the course of pre-straining (through the stress induced ε-α' transformation and variant-variant interaction), as has been observed in previous studies on Fe-Mn-Si-Cr-Ni alloys.[17,20,21] The shape recovery of the single-phase austenitic alloys remains almost unaffected till 5 pct Co addition, beyond which it improves. However, the highest amount of recovery, observed in the case of 9Co alloy, is still lower than that of the base alloy (alloy 0Co).

D. *Mechanical Properties*

In order to understand the shape recovery behavior of these alloys, room temperature tensile tests were conducted on specimens solution treated at 1323 K (1050 °C). Figure 7(a) presents the stress-strain curves

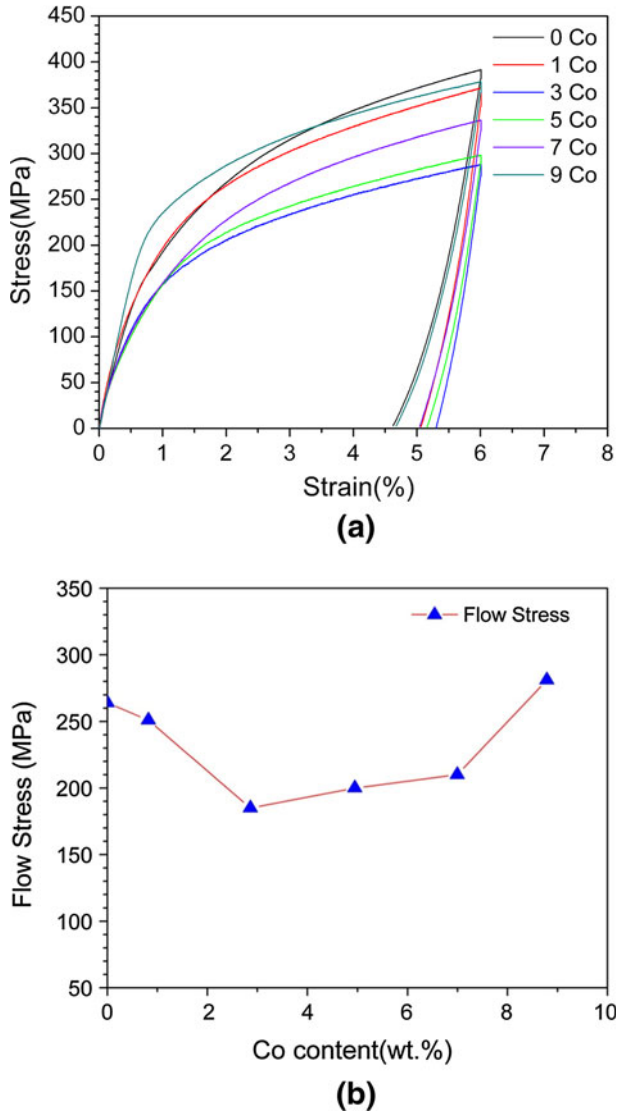

Fig. 7—(*a*) The stress-strain curves of 1323 K (1050 °C) solution annealed specimens obtained from tensile tests conducted at room temperature and (*b*) the variation of flow stress (at 1 pct strain) with Co addition. The flow stress of these alloys was observed to decrease till 3 pct Co and beyond that it increases.

obtained from tensile tests on specimens deformed up to 6 pct strain. Figure 7(b) shows that, initially, the flow stress (at 1 pct strain) decreases up to 3 pct Co content, beyond which it rises monotonically, possibly due to presence of $Fe_5Mn_3Si_2$ intermetallic precipitates within the two-phase microstructure. The results indicate that the deterioration of shape recovery in the single-phase γ alloys is related to the lower resistance to plastic yielding, and the improvement after 5 pct Co accrues from strengthening due to two-phase microstructure.

E. *Microstructure After Pre-straining*

The microstructural changes during pre-straining were investigated using tensile specimens deformed up to 6 pct strain. The amounts of stress induced martensite and

Table V. Volume Fraction of Parent and Martensite Phases After Pre-straining

Alloy	Volume Fraction of Phases (pct)		
	γ	ε	α'
0Co	51.26	47.19	1.55
1Co	35.00	62.38	2.62
3Co	52.92	44.94	2.14
5Co	48.13	48.37	3.50
7Co	37.39	62.61	–
9Co	27.80	72.20	–

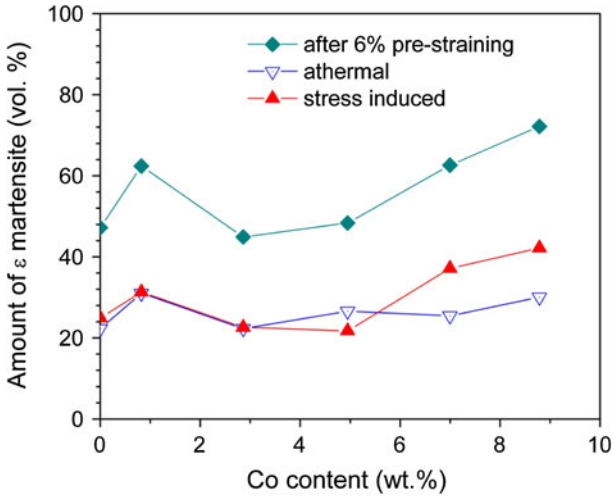

Fig. 8—The effect of Co addition on the amount of athermal and stress induced ε martensite.

other phases were estimated from the XRD patterns obtained from the gauge length portion of the specimens using quantitative Rietveld analysis[18] and are presented in Table V. It is seen that, the total amount of ε martensite increases after pre-straining, as expected, in proportion to the amount of stress induced phase created. The amount of stress induced ε martensites was estimated from the difference between the total amount of ε martensite after 6 pct pre-straining (Table V) and the amount of athermal ε martensite after solution annealing (Table II). As shown in Figure 8, the amount of stress induced ε martensite remains more or less the same till 5 pct Co and increases thereafter.

Table V also shows that the total amount of *bcc* phase (either δ-ferrite or α' martensite) presents has not changed much, even after 6 pct pre-straining. This clearly shows that, if at all, only a small insignificant amount of stress induced α' martensite may have formed during pre-straining. Figure 9 shows the optical micrographs obtained from the gauge length portion of the pre-strained specimens. It is seen that apart from the γ and ε martensite no other phase is present. EBSD phase maps generated from the gauge length portion, Figure 10, also corroborate this observation. Therefore, the formation of stress induced α' martensite in pre-straining is ruled out as a possible cause of the deterioration of shape recovery. An attempt was also made to identify the second-phase precipitate by EBSD mapping. As shown in the phase map of alloy 9Co, Figure 10(e), it was possible to successfully identify the precipitate at the grain boundaries to be the $(Fe,Co)_5Mn_3Si_2$ type intermetallic phase having a simple cubic structure with $P2_13$ space group and lattice parameter $a = 0.6135$ nm. On the basis of the chemical information (Section III–A) and the crystal structure identification by EBSD, we can conclude that the observed precipitates are that of the $(Fe,Co)_5Mn_3Si_2$ type intermetallic π-phase.

IV. DISCUSSION

The microstructural observations carried out in this study reveal that the microstructure of alloys containing 0 to 5 pct Co (alloys 0Co to 5Co) is a single-phase γ and that of alloys with more than 5 pct Co (*i.e.*, 6 to 9 pct Co) is a two-phase one consists of γ and $(Fe,Co)_5Mn_3Si_2$ type intermetallic phase. The observation of $(Fe,Co)_5Mn_3Si_2$ type intermetallic phase, which is isostructural with the π-phase ($Ni_5Cr_3Si_2$) found in Cr-Ni-Si alloy system in the range of 1123 K to 1448 K (850 °C to 1175 °C),[22] is reported here for the first time in the Fe-Mn-Si-Co alloy system. The existence of stoichiometric $Fe_5Mn_3Si_2$ and off-stoichiometric $Fe_5(Ni,Mn,Cr)_3Si_2$ intermetallic precipitates have been previously observed in the range of 973 K to 1223 K (700 °C to 950 °C) in Fe-Mn-Si and Fe-Mn-Si-Cr-Ni SMA systems.[23,24] In the present study, the off-stoichiometric $(Fe,Co)_5Mn_3Si_2$ intermetallic phase was observed after solution annealing at 1323 K (1050 °C) temperature. Therefore, it appears that the addition of Co has extended the stability of this phase to a higher temperature. Our previous investigations have shown that the stability of π-phase can be increased by the addition of Si or Cu.[17,25] The importance of π-phase in the present work is that it contributes to the improvement of shape recovery by counteracting the deleterious effect of Co. The following discussion is on determining the reasons why Co has proved to be harmful for the shape recovery of Fe-Mn-Si alloys.

Based on an understanding of the factors that contribute towards improving shape recovery, its deterioration can be said to be on account of the following causes: (i) higher plastic yielding of the γ matrix, (ii) relatively higher stacking fault energy and (iii) augmented formation of stress-induced α' martensite. The general deterioration of shape recovery with pre-strain is related to the formation of strain induced "window type" α' martensite at the junctions of interacting ε martensite variants.[20,21] The window martensite, which usually forms at pre-strains higher than 2 pct, acts as effective barriers to the reversible motion of Shockley partials involved in shape recovery.[20,21] While this is true for all Fe-based SMA, the mechanism (iii) listed above concerns the loss of memory on account of α' martensite induced by the ε-α' transformation during pre-straining. Two good examples of this are found in Fe-Mn-Si-Cr-Ni and Fe-Mn-Si-Ni-Cr-N alloys.[17,26] In

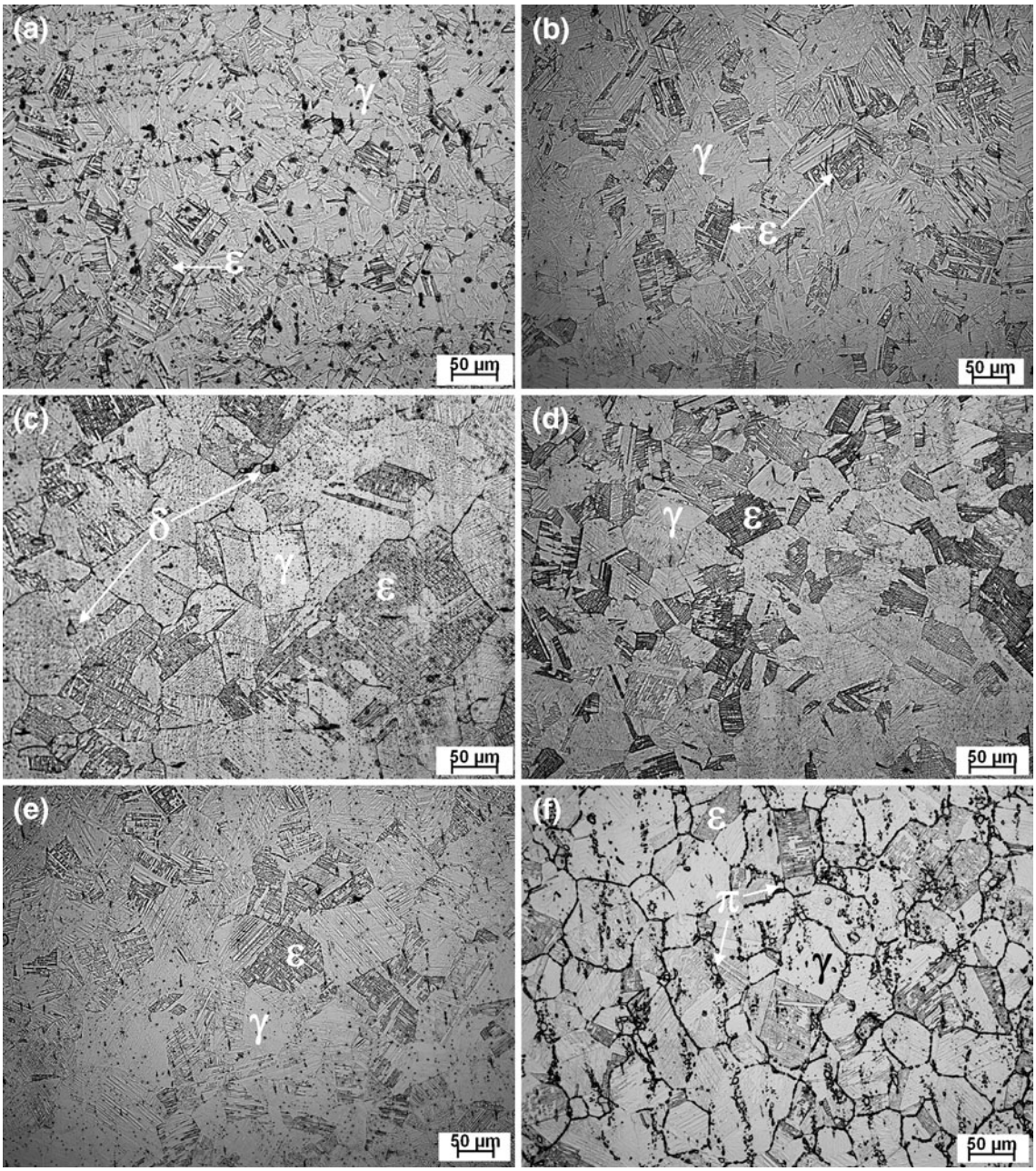

Fig. 9—Optical micrographs obtained after 6 pct pre-straining from specimens of (*a*) 0Co, (*b*) 1Co, (*c*) 3Co, (*d*) 5Co, (*e*) 7Co and (*f*) 9Co alloys reveal the formation of stress induced ε martensite during pre-straining. Formation of stress induced α′ martensite through γ-ε-α′ route has not been noticed in these alloys while pre-straining. However, presence of a few discrete δ-ferrite particles could be noticed in alloy 3Co (c).

Fe-Mn-Si-Cr-Ni alloys for instance, alloys with Si < 4 pct show poor shape recovery on account of ε-α′ transformation and in alloys with higher Si, the memory is greatly improved with the martensite-martensite transformation being suppressed.[17] In the present study, however, microstructural investigations using optical microscopy, EBSD and XRD clearly show that Co addition does not cause the formation of stress induced α′ martensite in Fe-Mn-Si alloys. Therefore, the cause of the deterioration of shape recovery could either be (i) or (ii) listed above.

It is well known that the variation of SFE with alloy addition provides an insight into the nature of the associated martensitic transformation. In the present work, the stacking fault probability in alloys 0Co-9Co was obtained using the Warren-Averbach technique of X-ray line profile analysis.[27] The SFE were then estimated from the observed magnitudes of the stacking fault probability using the relationships provided by Schramm and Reed.[28] As the data for the shear modulus along (111) plane (usually measured in single-crystals) was not available for this alloy system, it was assumed to be equal to that of the 'isotropic' modulus of polycrystalline material. Figures 11(a) and (b) shows the isotropic shear modulus, G, and the SFE calculated using the relationships given by Ghosh and Olson[29]

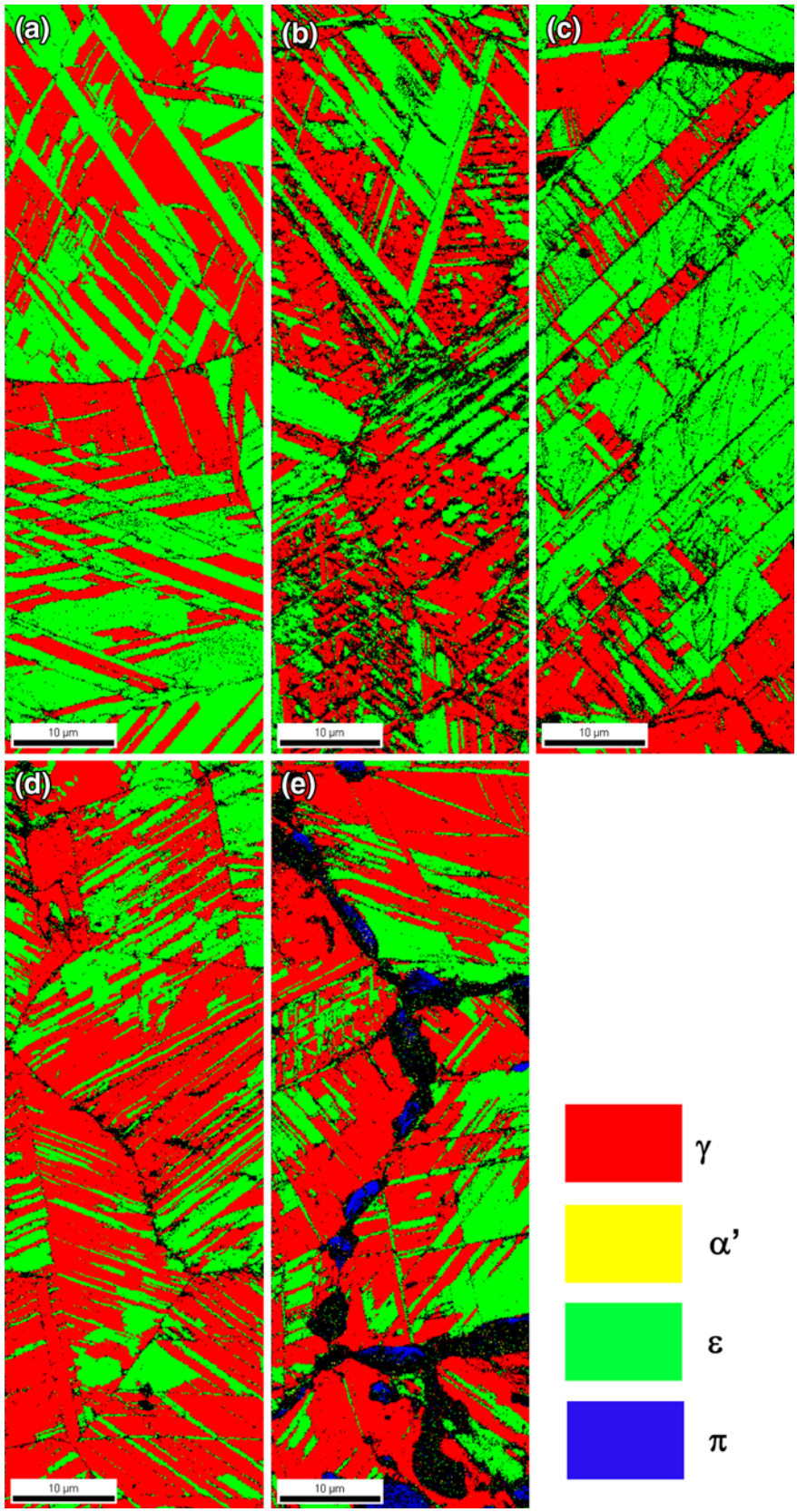

Fig. 10—EBSD phase maps generated from alloys (*a*) 0Co, (*b*) 1Co, (*c*) 3Co, (*d*) 7Co and (*e*) 9Co after 6 pct pre-straining show only the presence of γ (red areas) and stress induced ε martensites (green regions). Presence of stress induced α' martensite has not been seen in these microstructures. The phase map obtained from alloy 9Co (e) also reveals the existence of π-phase intermetallic precipitates (blue regions) along the grain boundaries (Color figure online).

and Schramm and Reed,[28] respectively. It can be seen that, Figure 11(a), the magnitude of G largely remains unaffected by Co addition. On the other hand, as seen in Figure 11(b), alloying with Co leads to a substantial decrease in the SFE. In general, it has been observed that Co reduces the SFE of austenitic stainless steels.[30,31] More recently, quantum-mechanical first principles calculations carried out by Lu *et al.*[32] establish that hcp stabilizers like Co always decrease the SFE of Fe-Cr-Ni austenitic alloys. A similar effect has also been observed in Fe-Mn-Co austenitic alloys. Here, the addition of Co has been reported to cause the decrease of T_N and SFE.[14,33,34] The important point to be noted is that shape recovery deteriorates with Co addition, though SFE decreases. While this effectively rules out mechanism (ii) listed earlier on, a more detailed analysis is necessary to rationalize the behaviour.

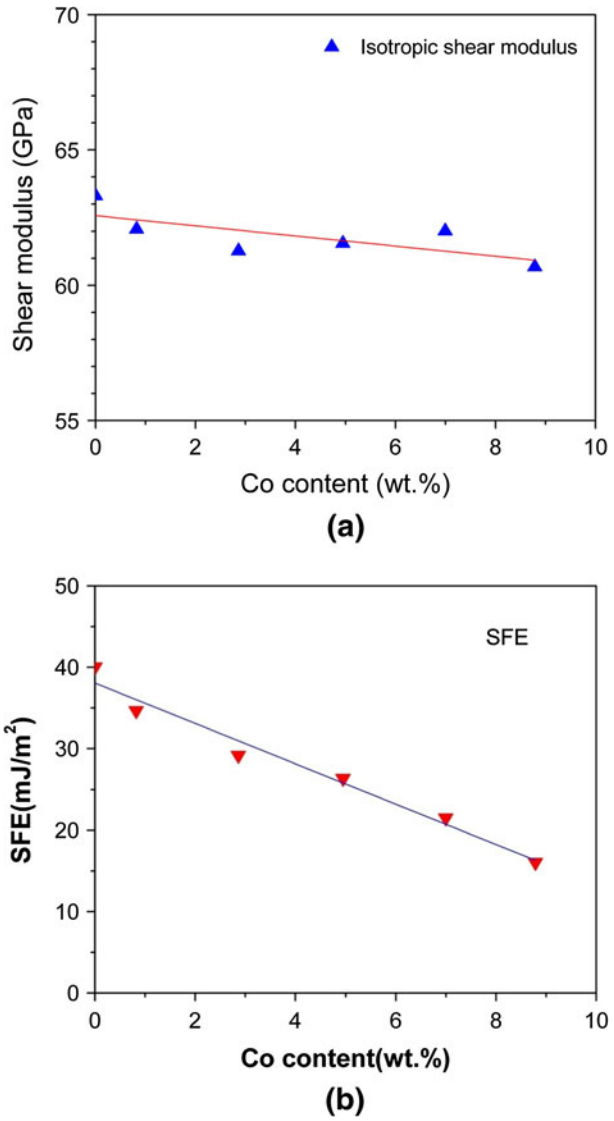

Fig. 11—Addition of Co to Fe-Mn-Si alloys does not significantly affect the shear modulus (*a*) of these alloys. However, the stacking fault energy (*b*) decreases considerably due to Co addition.

The Olson and Cohen approach[35] for the calculation of the energy required for the nucleation of martensite can also be applied for determining stacking fault energy. Considering that stacking faults are two layers of the *hcp* phase in *fcc* matrix, the fault energy (Γ) for a fault comprising of n planes can be expressed, in terms of per unit area of the fault in the fault plane, as the sum of the chemical free energy difference between the parent and product phase (ΔG^{chem}), the strain energy (E^{str}) and the surface energy ($\sigma(n)$):

$$\Gamma(n) = n\rho A\left(\Delta G^{chem} + E^{str}\right) + 2\sigma(n) \qquad [1]$$

Here, ρA = density of atoms in a close packed plane in moles per unit area and $n = 2$.

Previous studies[35] have demonstrated that the coherency strain energy (E^{str}) is less than 0.1 pct of the measured fault energy associated with the γ-ε transformation. If we add to this the observation that the shear modulus (which is related to E^{str}) of Fe-Mn-Si alloys is largely constant and unaffected by Co addition, Figure 11(a), it strongly suggests that the contribution of the coherency strain energy to the SFE is negligible. This, perhaps, is applicable to all alloy systems showing the γ-ε transformation. On the other hand, at temperatures higher than the Ms temperature of the γ-ε transformation, the absolute magnitude of the surface energy contribution to SFE is more than that of the chemical free energy. A survey of the published literature[35,36] indicates that this difference can be considerable, up to nearly twice as much at M_S. For instance, the work of Olson and Cohen,[35] in which surface and chemical free energies for Fe-Cr-Ni alloys were calculated from the SFE data measured by Lecroisey and Pineau,[37] it is seen that the absolute magnitude of these parameters are in the range of 10 to 12 mJ/m^2 and 3 to 4 mJ/m^2, respectively. Similar values for Fe-Mn alloys are obtained from the work of Coates *et al.*,[36] who have used the SFE data measured by Schumann[38] and Volosevich *et al.*,[39] *i.e.*, 16 to 19 mJ/m^2 and 8 to 10 mJ/m^2, respectively. In any case, it can be safely stated that surface energy and chemical free energy are the major contributors to the SFE in these alloy systems.

The change in the chemical free energies for the γ-ε transformation can be estimated from the change in the T_0 temperature, *i.e.*, the temperature at which free energies of the γ and ε phases are equal. In non-thermoelastic alloys T_0 is defined to be equally distant from the M_S and the A_S temperatures, *i.e.*, $T_0 = (A_S + M_S)/2$. In this sense, M_S and A_S correspond to 'supercooling' or hysteresis of the forward transformation, $T_0 - M_S$, and 'superheating' or hysteresis of the reverse transformation, $A_S - T_0$. Figure 5 and Table IV show that A_S of the γ-ε transformation is not affected by Co addition, and only M_S is. The latter decreases up to 5 pct Co addition and increases thereafter. In other terms, the $A_S - M_S$ hysteresis initially increases with Co addition and decreases when the alloy enters the two phase ($\gamma + \pi$-phase) region. The observed constancy of the A_S temperature strongly suggests that the T_0

temperature is also unaffected by Co addition. This behavior has been previously observed by Baruj *et al.*,[16] in their study on thermodynamic modeling of the γ-ε transformation in Fe-Mn-Co alloys. It was seen that the T_0 temperatures of Fe-Mn-Co alloys containing more than 25 pct Mn remains almost unchanged, even when Co is varied from 0 to 10 pct. Apart from this fact, the variation of T_0 can also be discerned from the change in amount of athermal martensite formed. In our previous studies on Fe-Mn-Si-Cr-Ni-N alloys[26] and Fe-Mn-Si-Cr-Ni-Cu alloys,[25] it was clearly seen that the amount of athermal ε martensite decreases with T_0. This behaviour is related to the fact that increased stability of that parent phase is reflected in T_0 and amount of athermal martensite. In the present study, however, the amount of athermal martensite was determined to be more or less constant across the composition range, which, therefore, suggests that the T_0 temperature remains unchanged. Further support for this suggestion comes from the observed variation of transformation temperature with SFE.[40,41] The works of Jun and Choi[40] on Fe-Mn alloys and Jiang and Qi[41] on Fe-Mn-Si alloys show that M_S increases with reduction in SFE. This can be explained on the basis of the fact that increased stability of martensite is indicated in both M_S and SFE. However, in the present study, contrary to this expectation, the M_S temperature decreases with Co addition. Thus, it can be said with a degree of certainty, that the T_0 temperature of Fe-Mn-Si alloys is unaffected by alloying with Co and remains constant over the composition range 0 to 9 pct.

On the other hand, constancy of T_0 implies that the variation in the SFE of Fe-Mn-Si-Co alloys can be assigned only to the lowering of the stacking fault surface energy. Cotes *et al.*[36] made an attempt to estimate the surface energy contribution in Fe-Mn alloys from the SFE values measured by Schumann[38] at 298 K (25 °C). Their results reveal that addition of Mn causes a decrease in the surface energy of stacking faults. In a similar way, the decrease in SFE observed in this study is most likely to be on account of a reduction in the surface energy contribution. Yakubtsov *et al.*[42] have shown that N addition to Fe-Cr-Ni-Mn alloys significantly decreases the SFE through the surface energy contribution. In this case, however, the decrease in surface energy is primarily due to Suzuki segregation of N to the stacking faults. In the present case it is not clear as to how Co influences and reduces the surface energy contribution to SFE of Fe-Mn-Si alloys.

The analysis of the results of the present study shows that T_0 and not SFE is a better reflection of the transformation behavior as it singularly indicates available chemical driving force. A low SFE is appropriate for stress induced martensite only when it is associated with a high chemical driving force. In the present situation, the reduction in SFE is only on account of lower surface energy contribution and, therefore, it does not translate into more stress induced martensite or increased shape recovery. It also appears that the lower surface energy does not translate into higher potency of embryos as the volume fraction of athermal martensite is almost constant.

Delaey *et al.*[43] have argued that transformation hysteresis is always related to energy dissipative processes. They have suggested that the main components of the dissipative process in thermoelastic transformations are: (i) resistance to interfacial motion, (ii) local relaxation of elastic strain energy, (iii) aging and stabilization and (iv) adiabatic interfacial motion. The first component relates to the energy required to overcome the frictional resistance to the interfacial motion, the second and third components relate to the loss of driving force on account of relaxation of the stored elastic energy and aging or stabilization behavior and the last component relates to the loss of driving force on account of the effects of rise or fall in temperature due to rapid movement of transforming front. In non-thermoelastic martensites of Fe-based shape memory alloys components (ii) and (iii) are not relevant and any contribution from component (iv) is not expected to change with alloying. Thus it is obvious that only component (i) is of significance to the non-thermoelastic martensitic transformations in Fe-based SMAs. A shear stress is required to overcome the resistance to interface motion and accomplish the transformational shear strain. Then, the shear stress times the shear strain is the frictional work dissipated in moving the martensite interface.[44] The frictional work will oppose both forward and reverse transformations. However, differences in the frictional resistance to the forward and reverse transformations will cause asymmetry in the position of T_0 with respect to M_S and A_S. As it was reasoned earlier on that T_0 of these alloys does not change with Co addition, it implies that the dissipative processes corresponding to $T_0 - M_S$ and that corresponding to $A_S - T_0$ are unequal in magnitude. Thus, the observed behavior of M_S and A_S can be explained as follows: that frictional loss in the reverse ε-γ transformation remains constant over composition, while that in the forward γ-ε transformation increases till 5 pct Co and reduces thereafter.

Olson and Cohen[45] argued that heterogeneous semicoherent nucleation can occur spontaneously only when the negative fault energy balances the interfacial frictional work. The driving force required for such nucleation is obtained from cooling or applied stress. Assuming a fixed defect potency, the critical driving force ($-\Delta G_{crit}$) has been expressed as follows[46]:

$$-\Delta G_{crit} = E^{str} + (2\sigma/nd) + W_\mu + W_{th} \qquad [2]$$

where E^{str} is molar strain energy and n is the number of closed-packed planes comprising the nucleus thickness; d is the spacing between closed-packed planes; σ is the semicoherent interfacial energy; W_μ and W_{th} are the athermal (composition dependent) and thermal (temperature and composition dependent) components of the interfacial frictional work, respectively. When W_{th} is negligible, the critical driving force is mainly influenced by compositional dependent W_μ. Ghosh and Olson[46] modeled W_μ of the γ-α' martensitic transformation in multi-component Fe-alloys and showed that, unlike other alloying elements, Co has a tendency to reduce the interfacial frictional work. Thus, the well known behav-

ior of Co, which is that it raises M_S of γ-α' transformation, is attributed to the reduction in the driving force for nucleation brought about by a reduction in the interfacial frictional work. In light of the observations made in the present work it can be stated that, in Fe-Mn-Si alloys, Co increases the athermal interfacial frictional work, W_μ, of the γ-ε transformation. The nature of this frictional work reveals itself in the mechanical behavior of these alloys.

The apparent flow strength of these alloys is related to the stress required for the nucleation of martensite and the plastic yielding of austenite matrix. When the amount of plastic yielding is less, the apparent flow stress corresponds to the stress to nucleate martensite and, therefore, increases with decreasing M_S, and *vice versa*. However, in the present study, the flow stress decreases with M_S, up to 5 pct Co addition, and thereafter increases along with M_S. This clearly indicates that, in Fe-Mn-Si-Co alloys, plastic yielding is the major component governing the observed deformation behavior. The other point is that lower SFE should have resulted in higher resistance to plastic deformation, unlike what has been observed in the present study. This fact suggests that the plastic yielding in Fe-Mn-Si-Co alloys is inhomogenous and concomitant with the formation of stress induced martensite. It is this last point that is of the highest significance as it seen (in this work) to result in poor shape recovery. Though, in alloys with Co up to 5 pct, almost the same amount of stress induced martensite forms during pre-straining, the difference in the extent of concomitant plastic yielding results in different extents of shape recovery. Hamers and Wayman[12] also concluded that the low shape recovery of Fe-Mn-Co SMAs is on account of the lower strength of the matrix, although, their study did not provide experimental evidence of the same. Beyond 5 pct Co addition, on the other hand, when the microstructure is composed of γ and π-phase, the added resistance to concomitant plastic yielding, which manifests as a rise in M_S and as an increase in the amount of stress induced ε martensite, results in the improvement of the shape recovery. The manner in which the concomitant plastic yielding results in poor shape recovery was, however, difficult to discern.

V. CONCLUSIONS

The important conclusions based on the observations made in this study can be summarized as follows:

1. In Fe-Mn-Si-Co alloys, the microstructure remains single-phase γ only up to 5 pct Co. Alloys containing more than 5 pct Co show a two-phase microstructure composed of γ and off-stoichiometric $(Fe,Co)_5Mn_3Si_2$ type intermetallic phases.
2. Cobalt addition decreases the resistance to plastic yielding. However, beyond 5 pct Co, increase in flow stress occurs due to the presence of $(Fe,Co)_5Mn_3Si_2$ precipitates. It appears that the plastic yielding in Co containing alloys is inhomogenous and concomitant with formation of stress induced martensite.
3. Cobalt addition up to 5 pct decreases the M_s temperature of the γ-ε transformation, although, the A_S temperature remains constant. It has been reasoned out that T_0 remains unaffected by alloying with Co. The asymmetric hysteresis, *i.e.*, unequal $A_S - T_0$ and $T_0 - M_S$, appears to be on account of differences in the athermal frictional work arising out of the concomitant plastic yielding.
4. Cobalt addition decreases the stacking fault energy of Fe-Mn-Si alloys. It has been reasoned out that this decrease is essentially due to the decrease in the surface energy contribution to SFE.
5. In general, addition of Co to Fe-Mn-Si alloys deteriorates shape recovery. However, when the Co > 5 pct, shape recovery improves due to the strengthening provided by the two-phase microstructure and higher amount of stress induced ε martensite.

ACKNOWLEDGMENTS

The authors are grateful to Prof. I. Samajdar and Mr. R. Basu, Indian Institute of Technology, Bombay, India for their help received during EBSD measurements. We would also like to thank Mr. V.C. Krishnamohan Nair and Mr. S. Yadav for their help received during melting and processing of alloys used in this study.

REFERENCES

1. K. Enami, A. Nagasawa, and S. Nenno: *Scripta Metall.*, 1975, vol. 9, pp. 941–48.
2. S. Cotes, M. Sade, and A. Fernández Guillermet: *Metall. Mater. Trans. A*, 1995, vol. 26A, pp. 1957–69.
3. E. Gartstein and A. Rabinkin: *Acta Melall.*, 1979, vol. 27, pp. 1053–64.
4. A. Sato, E. Chisima, K. Soma, and T. Mori: *Acta Metall.*, 1982, vol. 30, pp. 1177–83.
5. M. Murakami, H. Otsuka, H. Suzuki, and S. Matsuda: *Trans. ISIJ*, 1987, vol. 27, p. B-88.
6. H. Otsuka, M. Murakami, and S. Matsuda: *The Proceedings of the MRS International Meetings on Advanced Materials*, Tokyo, Japan, 1989, vol. 9, pp. 451–56.
7. K. Yamaguchi, Y. Morioka, and Y. Tomota: *Scripta Mater.*, 1996, vol. 35, pp. 1147–52.
8. H. Otsuka, H. Yamada, H. Tanahashi, and T. Maruyama: *Mater. Sci. Forum*, 1990, vols. 56–58, pp. 655–60.
9. K. Tsuzaki, Y. Natsume, Y. Kurokawa, and T. Maki: *Scripta Metall.*, 1992, vol. 27, pp. 471–73.
10. L. Jian and C.M. Wayman: *Mater. Charact.*, 1994, vol. 32, pp. 215–27.
11. A. Ariapour, I. Yakubtsova, and D.D. Perovic: *Metall. Mater. Trans. A*, 2001, vol. 32A, pp. 1621–28.
12. A.A.H. Hamers and C.M. Wayman: *Scripta Metall.*, 1991, vol. 25, pp. 2723–28.
13. M.M. Reyhani, X. Chen, and P.G. McCormick: *Proceedings of the International Conference on Martensitic Transformations (ICOMAT-1992)*, Monterey, California, 1992, pp. 1163–68.
14. B. Jiang, K. Xu, X. Qi, and W. Zhou: *J. Phys. IV*, 2003, vol. 112, pp. 393–96.
15. A. Baruj, A. Fernández Guillermet, and M. Sade: *J. Phys. IV*, 1995, vol. 5, pp. C8-373–C8-378.
16. A. Baruj, A. Fernández Guillermet, and M. Sade: *J. Phys. IV*, 1997, vol. 5, pp. C5-405–C5-410.
17. B.C. Maji, M. Krishnan, Gouthama, and R.K. Ray: *Metall. Mater. Trans. A*, 2011, vol. 42A, pp. 2153–65.

18. H.M. Rietveld: *Acta. Crystallogr*., 1967, vol. 22, pp. 151–52.
19. U. Sari and T. Kirindi: *Mater. Chem. Phys*., 2011, vol. 130, pp. 738–42.
20. J.H. Yang and C.M. Wayman: *Metall. Trans. A*, 1992, vol. 23A, pp. 1445–54.
21. B.C. Maji and M. Krishnan: *Scripta Mater*., 2003, vol. 48, pp. 71–77.
22. P. Villers, A. Prience, and H. Okamoto: *Handbook of Ternary Alloy Phase Diagram*, 1st ed., ASM, Metals Park, OH, 1995, vol. 3, pp. 9147–49.
23. P. Villers, A. Prience, and H. Okamoto: *Handbook of Ternary Alloy Phase Diagram*, 1st ed., ASM, Metals Park, OH, 1995, vol. 3, pp. 10427–38.
24. B.C. Maji, M. Krishnan, and V.V. Rama Rao: *Metall. Mater. Trans. A*, 2003, vol. 34A, pp. 1029–42.
25. B.C. Maji, M. Krishnan, Gouthama, and R.K. Ray: unpublished research.
26. B.C. Maji and M. Krishnan: *Proceedings of the International Conference on Martensitic Transformations (ICOMAT-2008)*, Santa Fe, New Mexico, 2008, pp. 349–57.
27. B.E. Warren and B.L. Averbach: *J. Appl. Phys*., 1950, vol. 21, pp. 595–99.
28. R.E. Schramm and R.P. Reed: *Metall. Trans. A*, 1975, vol. 6A, pp. 1345–51.
29. G. Ghosh and G.B. Olson: *Acta Mater*., 2002, vol. 50, pp. 2655–75.
30. F.B. Pickering: *Physical Metallurgy and Design of Steels*, Applied Science Publication Ltd., London, U.K., 1978, p. 238.
31. H.K.D.H. Bhadeshia and R.W.K. Honeycombe: *Steels Microstructure and Properties*, 3rd ed., Butterworth-Heinemann, Oxford, 2006, p. 283.
32. S. Lu, Q. Hu, B. Johansson, and L. Vitos: *Acta Mater*., 2011, vol. 59, pp. 5728–34.
33. M. Murakami, H. Otsuka, H.G. Suzuki, and S. Matsuda: *Proceedings of the International Conference on Martensitic Transformations (ICOMAT-86)*, Sendai, Japan, 1986, p. 985.
34. T. Maki: in *Shape Memory Materials*, K. Otsuka and C.M. Wayman, eds., Cambridge University Press, Cambridge, U.K., 1999, pp. 117–32.
35. G.B. Olson and M. Cohen: *Metall. Trans. A*, 1976, vol. 7A, pp. 1897–1904.
36. S. Cotes, A. Fernández Guillermet, and M. Sade: *Metall. Mater. Trans. A*, 2004, vol. 35A, pp. 83–91.
37. F. Lecroisey and A. Pineau: *Metall. Trans. A*, 1972, vol. 3A, pp. 387–96.
38. H. Schumann: *J. Kristall Technik*, 1974, vol. 10, pp. 1141–50.
39. P.Y. Volosevich, V.N. Gridnev, and Y.N. Petrov: *Fiz. Met. Metalloved*., 1976, vol. 42 (2), pp. 126–30.
40. J. Jun and C. Choi: *Mater. Sci. Eng*., 1998, vol. A257, pp. 353–56.
41. B. Jiang and X. Qi: *Bull. Mater. Sci*., 1999, vol. 22, pp. 717–21.
42. I.A. Yakubtsov, A. Ariapour, and D.D. Perovic: *Acta Mater*., 1999, vol. 47, pp. 1271–79.
43. L. Delaey, J. Ortin, and J. Van Humbeeck: *Proceedings of the International Conference on Solid-Solid Phase Transformation*, Cambridge, U.K., 1987, pp. 60–66.
44. G.B. Olson and M. Cohen: *Scripta Metall*., 1977, vol. 11, pp. 345–47.
45. G.B. Olson and M. Cohen: *Metall. Trans. A*, 1976, vol. 7A, pp. 1915–23.
46. G. Ghosh and G.B. Olson: *Acta Metall. Mater*., 1994, vol. 42, pp. 3361–70.